

Highlights

A comprehensive guide for measuring total vanadium concentration and state of charge of vanadium electrolytes using UV-Visible spectroscopy

Ange A. Maurice, Alberto E. Quintero, Marcos Vera

- UV-Visible spectroscopy is used to characterize vanadium electrolytes.
- Three electrolyte solutions relevant to vanadium redox flow batteries are studied: the anolyte V^{II}/V^{III} , the catholyte V^{IV}/V^{V} , and the intermediary electrolyte V^{III}/V^{IV} .
- A fast empirical method and a method based on spectral deconvolution are proposed for each electrolyte.
- The proposed methods are calibrated over a wide range of concentrations (0.91-1.83M).
- Total vanadium concentration and state of charge can be accurately measured.
- Overall accuracy is 25-35 mM for the concentration and 1.0-1.5% for the state of charge.

A comprehensive guide for measuring total vanadium concentration and state of charge of vanadium electrolytes using UV-Visible spectroscopy

Ange A. Maurice^{a,*}, Alberto E. Quintero^{a,b}, Marcos Vera^a

^aDepartamento de Ingeniería Térmica y de Fluidos, Universidad Carlos III de Madrid, Avd. de la Universidad 30, Leganés, 28911, Madrid, Spain

^bR&D Department, Micro Electrochemical Technologies, Leganés, 28918, Madrid, Spain

Abstract

This paper presents an exhaustive how-to guide on measuring the total vanadium concentration and state of charge of vanadium electrolytes using UV-Visible spectroscopy. The study is provided with an open-access database (GitHub) that supports the methods and procedures and facilitates access to the calibration data. The study covers the three types of electrolyte solutions relevant to vanadium redox flow batteries, namely the anolyte V^{II}/V^{III} , the catholyte V^{IV}/V^{V} , and the V^{III}/V^{IV} commercial electrolyte, meant to be preconditioned to either V^{III} or V^{IV} before battery operation. Analytical expressions to calculate the concentration of different vanadium species in the electrolyte solutions are provided based on either empirical correlations or spectral deconvolution methods. The paper also examines the limitations of the measurement technique and provides insightful recommendations for future research. The open-access database provided by the authors is expected to serve as a valuable repository for scholars and scientists working in the field of vanadium redox flow batteries.

Keywords: UV-Vis spectroscopy, Vanadium electrolytes, Calibration methods, Concentration, State of charge, Redox flow batteries

1. Introduction

The rapid growth of renewable energy sources as a sustainable alternative to traditional power generation requires the development of effective energy storage solutions capable of mitigating the power grid fluctuations inherent to clean energy technologies [1]. In this context, vanadium redox flow batteries (VRFBs) offer several advantages that make them a promising large-scale stationary energy storage solution: high round-trip energy efficiency, excellent scalability, long cycle life, decoupled power and energy capacity, deep discharge capability, and high safety compared to other types of batteries. These advantages posit VRFBs as a promising energy storage technology for various applications, including grid-level energy storage, renewable energy integration, load balancing, and backup power systems. However, VRFBs also face challenges such as lower energy

*Corresponding author

Email addresses: amaurice@uc3m.es (Ange A. Maurice), marcos.vera@uc3m.es (Marcos Vera)

and power density, high cost, complex system design, electrolyte degradation, and environmental concerns [2, 3, 4].

In particular, one of the main drawbacks of VRFBs is their capacity decay during cycling, mainly caused by ion crossover [5], hydrogen evolution [6], or imperfect electrolyte mixing in the tanks [7]. This makes the total vanadium concentration and the state of charge (SOC) to drift away from symmetry between the negative and positive sides, creating a charge imbalance. To address and correct these issues effectively, real-time monitoring of the total vanadium concentration and SOC of the positive and negative half-cells would be highly desirable. Upon charge and discharge, the absorbance spectra of vanadium compounds vary significantly. Thus, a direct, non-invasive method to measure the SOC is through Ultraviolet-Visible (UV-Vis) absorbance spectroscopy.

The method comes as a valuable alternative to the classical approach of open circuit voltage (OCV) measurements, typically conducted offline in a smaller electrochemical cell separate from the main redox reactor. These OCV sensors are considered invasive due to the potential for crossover and self-discharge through the membrane of the smaller cell. Moreover, they are susceptible to temperature variations, and their measurement accuracy heavily depends on the precise design and operation of the cell to mitigate issues such as mass transfer limitations, preferential paths, or shunt currents, among others. Moreover, OCV measurements solely provide information about the overall SOC of the VRFB system, lacking the ability to determine the individual SOC of each electrolyte (positive and negative). Additionally, they do not provide insights into the total Vanadium concentration in each stream [8, 9].

More recent approaches, such as the online monitoring of density or viscosity to establish their correlation with the state of charge (SOC), still have limitations, including temperature dependency and the introduction of an additional pressure drop. These factors contribute to a decrease in the overall round-trip efficiency of VRFBs [10, 11]. In the case of membraneless redox flow batteries, which have gained significant research attention, an optical non-invasive measurement becomes crucial due to the limitations associated with the aforementioned methods. Furthermore, in membraneless systems, the simultaneous measurement of SOC and the total vanadium concentration in both electrolytes is required due to the absence of a membrane. Specifically, for micro membraneless VRFBs, it is imperative to minimize the dead volume in the microsensor, a challenge effectively addressed through non-invasive optical methods [12, 13]. Overall, optical sensors enable monitoring VRFB performance and provide more profound insights into the specific processes that control efficiency and capacity decay during operation, offering optimal real-time readings and enabling closed-loop control strategies [14, 15].

In the literature, the UV-Vis spectroscopy method has been extensively studied [16, 17, 18, 19], uncovering early the complex chemistry of the positive electrolyte with Blanc et al. [20] and more recently with Buckley et al. [21, 22, 23, 24]. Experimental tests have also been conducted using the UV-Vis method to determine the state of charge (SOC) both offline [25, 24] and online/in-operando [26, 27, 28]. However, upon browsing the extensive literature on the subject, a critical question still emerges: How can the total vanadium concentration and the SOC of both electrolytes in a VRFB be independently measured using UV-Vis spectroscopy, and what level of accuracy can be achieved with this method? While partial answers can be found in scattered publications, the available information often focuses solely on one specific electrolyte and lacks detailed analysis. In addition, certain reported calibrations only provide the SOC as an output, disregarding the total vanadium concentration. Moreover, limited information is available regarding measurement errors,

making it difficult to evaluate the robustness of the reported calibration methods. Furthermore, existing studies often present calibrations for a narrow range of concentrations.

To effectively address these knowledge gaps, the primary objective of this article is to present a comprehensive document that outlines calibration methods capable of accurately quantifying both the total vanadium concentration and the SOC across all possible vanadium electrolyte mixtures, encompassing a wide concentration range of 0.91 to 1.83 M. Moreover, we provide significant calibration improvements compared with the existing literature, resulting in better accessibility for the reader and improved measurement accuracy.

This study deals with the three types of vanadium electrolyte mixtures employed in VRFBs: *i*) the anolyte V^{2+}/V^{3+} (V^{II}/V^{III}), *ii*) the V^{3+}/VO_2^+ (V^{III}/V^{IV}) mixture and *iii*) the catholyte VO^{2+}/VO_2^+ (V^{IV}/V^{V}). Following standard practice, the four oxidation states of vanadium are denoted here V^{II} , V^{III} , V^{IV} , and V^{V} . During normal VRFB operation, the V^{III}/V^{IV} electrolyte should not be present and is typically less relevant. Nonetheless, a failing VRFB with high electrolyte imbalance could overdischarge and result in V^{III}/V^{IV} appearing in one of the tanks. Moreover, commercial vanadium electrolyte is usually distributed as an equimolar V^{III}/V^{IV} mixture, often referred to as V3.5+, meant to undergo a preconditioning process to achieve zero SOC either as anolyte or catholyte. Other vanadium electrolyte mixtures cannot exist since self-discharge reactions would occur yielding one of the three composition pairs indicated above [29].

For each electrolyte we provide two calibration methods: *i*) a fast empirical method based on linear regression, which requires only one or two hand-picked absorbances as input, and *ii*) a more computationally intensive method based on spectral deconvolution [30], which uses the whole spectrum as input. The methods to be outlined below are based on the generalized Beer-Lambert law. This law states that the total absorbance of a mixture containing multiple absorbing compounds is equal to the sum of the individual absorbances contributed by each compound. This principle assumes that the absorbing compounds in the mixture do not interact with each other and that their absorbance contributions are independent [31, 32, 33].

The calibration methods yield the total vanadium concentration C and the mole fractions X_i for the three electrolyte mixtures under study. In the case of the V^{II}/V^{III} and V^{IV}/V^{V} mixtures, anolyte and catholyte, the calibration also provides the SOC, represented by the mole fractions X_2 and X_5 , which is the desired piece of information for most readers. Table 1 defines the notation used in this paper, relating the total vanadium concentration C , the mole fractions X_i , and the SOC to the molar concentrations C_i of the four vanadium ions, $i = \{2, 3, 4, 5\}$. Note that in the V^{IV}/V^{V} mixture we include the presence of the 1:1 stoichiometric mixed-valence complex $V_2O_3^{3+}$ in equilibrium with V^{IV} and V^{V} according to reaction (9), whose concentration is denoted by subscript $i = 45$ [20]. Hereafter, the SOC and mole fractions are expressed as percentages unless otherwise stated.

The data set and the Python calibration algorithms generated in this work are publicly shared in an online repository (GitHub). We believe this decision will be helpful for both the scientific community and the industry. In general, adopting an open data approach proves most valuable in advancing the field, as it allows anyone to enhance the existing calibration procedures by employing more advanced chemometric techniques.

The paper is organized as follows. Section 2 describes the experimental procedures employed to prepare the calibration samples with the best accuracy. Section 3 presents the calibration methods for the different mixtures, starting with the anolyte V^{II}/V^{III} and the V^{III}/V^{IV} mixture,

which exhibit a common linear response. Subsequently, the calibration of the catholyte V^{IV}/V^V is discussed, showcasing its non-linear spectral response. In Section 4, we discuss the accuracy, advantages and disadvantages of the different methods. Finally, in Section 5 we summarize the key findings and draw the conclusions.

2. Experimental

2.1. Electrochemical preparation of the reference electrolytes

The calibration of UV-Vis spectroscopic methods requires the preparation of single-species reference electrolytes, and of mixtures thereof, with a high degree of compositional precision. In this section we describe the experimental procedures employed to generate these samples. We prepared the reference solutions of vanadium electrolytes via electrochemical reduction and oxidation in an in-house 3 cm^2 electrochemical cell. To avoid hydrogen evolution reactions and significant crossover effects, the applied cell voltage was kept at 1.6 V. Throughout the charge process, we acquired UV-Vis absorbance spectra periodically using flow cuvettes. As the starting electrolyte, we used an equimolar V^{III}/V^{IV} commercial solution (Oxkem Limited, UK) containing an average oxidation number (AOS) of +3.5. Its exact composition is listed in Table 2. Since all samples originated from this batch solution, we performed induction coupled plasma-optical emission spectroscopy (ICP-OES) to measure the total vanadium concentration with high accuracy, with the results given in the table. It is interesting to note that the solution contains 0.5 M of phosphoric acid, which is commonly used in commercial vanadium electrolytes to improve their solubility properties [34].

Slight variations of the total vanadium concentration can significantly affect the absorbance spectra measurements. This can occur, for instance, due to ion crossover across the membrane. To minimize such phenomenon, we stacked 3 layers of Nafion® N112 membrane following the

Variable	Electrolyte mixture		
	V^{II}/V^{III}	V^{III}/V^{IV}	V^{IV}/V^V
C	$C_2 + C_3$	$C_3 + C_4$	$C_4 + C_5 + 2C_{45}$
X_2	$\frac{C_2}{C_2 + C_3}$	—	—
X_3	$\frac{C_3}{C_2 + C_3}$	$\frac{C_3}{C_3 + C_4}$	—
X_4	—	$\frac{C_4}{C_3 + C_4}$	$\frac{C_4 + C_{45}}{C_4 + C_5 + 2C_{45}}$
X_5	—	—	$\frac{C_5 + C_{45}}{C_4 + C_5 + 2C_{45}}$
SOC	X_2	—	$X_5 = 1 - X_4$

Table 1: Definition of the total vanadium concentration C , molar fractions X_i , and SOC for the different electrolyte mixtures under study as a function of the molar concentration of the four vanadium ions C_i , $i = \{2, 3, 4, 5\}$. In the V^{IV}/V^V mixture C_{45} denotes the concentration of the 1:1 stoichiometric mixed-valence complex $V_2O_3^{3+}$ at equilibrium with V^{IV} and V^V according to reaction (9).

Species	Concentration
Vanadium	1.83 ± 0.092 M
Sulfuric Acid	4.6 M
Phosphoric Acid	0.5 M
Oxidation number	≈ 3.5

Table 2: Composition of the commercial vanadium electrolyte (Oxkem Limited, UK) used in the study, with an average oxidation number (AOS) of +3.5.

results published by Ashraf et al. [35]. With this membrane stacking and taking into account our charge duration of 5-15 hours, the total vanadium concentration should not vary more than 5 mM, which represents a variation of about 0.27%. Note that the calibrations and data shown in this paper are provided for a given acidity level. Minimal variations of spectrum shape could appear when varying the acidity [30]. However, given the small magnitude of these variations, we expect negligible impacts on the accuracy of the calibration. Additionally, the methodology presented in this paper remains valid regardless of the acidity and could be used to update the calibration for various acidic conditions, a potential research work that is outside the scope of this paper.

2.2. UV-Vis spectroscopy

We acquired the spectra using 0.1 mm and 1 mm path length commercial flow cuvettes (Starna Scientific Ltd., UK). Because of its lower absorption, we measured the V^{II}/V^{III} electrolyte using the 1 mm path length cuvette whilst for the other mixtures we used the 0.1 mm path length cuvette. The spectrometer (Flame T-VIS-NIR-ES, Ocean Insight, USA), the lamp (HL-2000-FHSA-LL, Ocean Insight, USA), and the cuvette holder (SQUARE ONE, Ocean Insight, USA) were connected via optical fibers. The Flame T-VIS-NIR-ES spectrometer has a wavelength detection range of 345-1033 nm and an optical resolution of 1.33 nm FWHM. However, considering the high absorbance of the electrolyte and the lamp emission range, the actual measurable range is about 420-1000nm depending on the concentration and the species. Upon measurement, we injected at least 1 mL of sample with a syringe in the flow cuvette in order to ensure ample clearing of the cuvette optical window. In this work, all absorbances are normalized with the optical path length, and thus their units are in cm⁻¹.

2.2.1. Preparation of V^{II} and V^V

The preparation of the charged V^{II} and V^V electrolyte solutions was achieved by starting from the equimolar V3.5+ solution and bringing the electrochemical oxidation and reduction of the electrolyte to completion. In other words, fully oxidizing or reducing the vanadium applying a fixed 1.6 V potential to the cell. The completion point was deemed to be reached when three independent criteria were met: *i*) the current density was lower than 2 mA/cm², *ii*) the UV-Vis spectrum remained stable for more than 10 min, and *iii*) the shape of the spectrum was coherent with previous literature results. It is worth noting that we had to increase the applied potential up to 1.7-1.8 V for a short period of time (10-15 min) to achieve a stable UV-Vis spectrum.

2.2.2. Preparation of V^{III} and V^{IV}

Similarly, we prepared the discharged V^{III} and V^{IV} electrolytes by electrochemical charging the equimolar V3.5+ solution. However, reaching the exact transition state, or endpoint, where only pure V^{III} or V^{IV} exist is more complex than for the fully charged electrolytes V^{II} and V^V. In this case, the use of online spectrometry is critical. The procedure, called spectrophotometric titration [33], consists in lowering the applied voltage or current when approaching the purity point and monitoring the spectra at specific wavelengths looking for an inflection point. Further elaboration on the procedure and specific criteria for its application to vanadium electrolytes can be found in the Supplementary Information (Figure S1). Obtaining V^{III} is relatively easier through this method, as an overcharge leads to the formation of V^{II}, which subsequently undergoes air oxidation. Indeed, when the negative electrolyte is exposed to air, it naturally tends to become pure V^{III}. Nevertheless, in order to prevent any potential impact on the total vanadium concentration due to water evaporation, efforts were made to minimize exposure to air.

2.2.3. Calibration samples

We prepared the calibration samples via pipetting and mixing/diluting of the reference solutions and a 4.6M sulfuric acid solution. The total sample volumes were 1-2 mL, depending on the desired vanadium concentration. Using deionized water and a 5-digit analytical weighing scale, we estimated the pipetting accuracy to be 0.4%. For each mixture, we prepared 11 samples at SOCs ranging from 0 to 100% and concentrations of 1.83, 1.52, 1.22, and 0.91 M (44 samples per mixture, 132 samples in total). We disregarded concentrations lower than 0.9 M for the calibration step since most industrial applications use electrolytes with concentrations higher than 1 M to maintain high capacity/volume ratios. Nonetheless, to verify the Beer-Lambert law, we additionally prepared samples with 0.6 and 0.3 M containing only pure compounds (see Section 3.1).

3. Results and calibration

3.1. Reference spectra

Figure 1a shows the reference absorbance spectra A_i of the single-species electrolyte solutions, obtained following the procedures outlined in section 2. The spectra A_2 , A_3 , A_4 , and A_5 correspond, respectively, to the oxidation states V^{II}, V^{III}, V^{IV}, and V^V. The shapes of the spectra are consistent with the visual appearance of the electrolytes depicted in Figure 1b, as well as the color band shown in Figure 1c. For instance, A_5 acts as a high-pass filter, suppressing the blue part of the visible spectrum and having negligible absorbance above 650 nm, which yields an orange/yellow color. By contrast, A_4 has very low absorption between 420-550 nm, resulting in a deep blue appearance. Figures 1d, 1e, 1f, and 1g show the measured absorbance as a function of the total vanadium concentration for the four vanadium oxidation states. The plots correspond to selected wavelengths, approximately aligned with the absorbance peaks depicted in Figure 1b for V^{II}, V^{III}, and V^{IV}, and at 440 nm for V^V, which lacks a well defined peak in the observed range. The linear fits (red dotted lines) obtained for V^{II}, V^{III}, and V^{IV} confirm the validity of the Beer-Lambert law

$$A_i = \epsilon_i C_i \quad \text{for } i = \{2, 3, 4\} \quad (1)$$

at least up to total vanadium concentrations of 1.83 M. In this expression A_i is the path-length normalized absorbance spectrum in cm^{-1} , C_i is the molar concentration in M, and ϵ_i represents the molar absorptivity (or molar absorption coefficient) of the i -th oxidation state, in $\text{cm}^{-1} \text{ M}^{-1}$.

By contrast, the relation between absorbance and concentration for V^V is non-linear, deviating from the classical Beer-Lambert law. This non-linear behavior can be effectively described by a power law equation of the form

$$A_5 = \epsilon_5 C_5^k \quad (2)$$

where the fitting exponent remains approximately constant for different wavelengths with a value of roughly $k \approx 2$, and ϵ_5 represents the molar absorptivity of V^V . The non-linear absorbance of V^V had been only briefly reported for V^V at ultra-low concentrations (< 0.03 M) by Bannard et al. [36]. Consequently, the deviation observed here at high concentrations is a novel result that, to the best of our knowledge, had not been previously reported in the literature. Non-linear deviations from the Beer-Lambert law at high concentrations may be due to different factors, such as intermolecular interactions or changes in the refractive index of the analyte. These deviations may result in complex spectral behaviors that cannot be accurately described by a simple linear relationship between absorbance and concentration [37, 38, 28].

The values of ϵ_i and k for the chosen wavelengths are annotated in the graphs of Figure 1 along with their corresponding statistical uncertainties given by the root mean square error (RMSE, or E in shorthand notation) between the predicted and the measured values. Table 3 lists values of the molar absorptivities ϵ_i for $i = \{2, 3, 4\}$ at selected wavelengths. As previously discussed, these wavelengths correspond to the local absorbance peaks of V^{II} , V^{III} , and V^{IV} , with the corresponding maxima of ϵ_i being highlighted in boldface in each case.

Wavelength	Electrolyte		
	V^{II}	V^{III}	V^{IV}
	ϵ_2	ϵ_3	ϵ_4
564 nm	4.36 ± 0.026	5.46 ± 0.079	2.91 ± 0.043
605 nm	3.21 ± 0.020	7.40 ± 0.053	7.18 ± 0.061
766 nm	2.11 ± 0.014	negligible	19.72 ± 0.095
850 nm	3.18 ± 0.032	negligible	10.82 ± 0.19

Table 3: Values of the 1.83 M molar absorptivities ϵ_i for $i = \{2, 3, 4\}$ at selected wavelengths determined by the local maxima of the absorbance curves of V^{II} , V^{III} , and V^{IV} . All units are in $\text{cm}^{-1}\text{M}^{-1}$.

The following sections provide detailed information about the spectral responses of the mixtures V^{II}/V^{III} , V^{III}/V^{IV} , and V^{IV}/V^V . While the V^{II}/V^{III} and V^{III}/V^{IV} mixtures show a linear response, the catholyte V^{IV}/V^V exhibits a non-linear response. This non-linear behavior is attributed both to the non-linear absorbance of V^V and to the formation of a high absorbance 1:1 stoichiometric complex between V^{IV} and V^V [20]. Consequently, the calibration methods for the three electrolyte mixtures are presented in two distinct sections addressing the linear and non-linear cases separately.

3.2. Linear case: V^{II}/V^{III} and V^{III}/V^{IV}

Figures 2a and 2b show, respectively, the molar absorptivity spectra of the V^{II}/V^{III} and V^{III}/V^{IV} mixtures at varying SOCs, or mole fractions, for a total vanadium concentration $C = 1.83$ M. The former electrolyte is characterized by the mole fraction of V^{II} , or X_2 , which coincides with the SOC, while the later is characterized by the mole fraction of V^{IV} , or X_4 . The vertical arrows

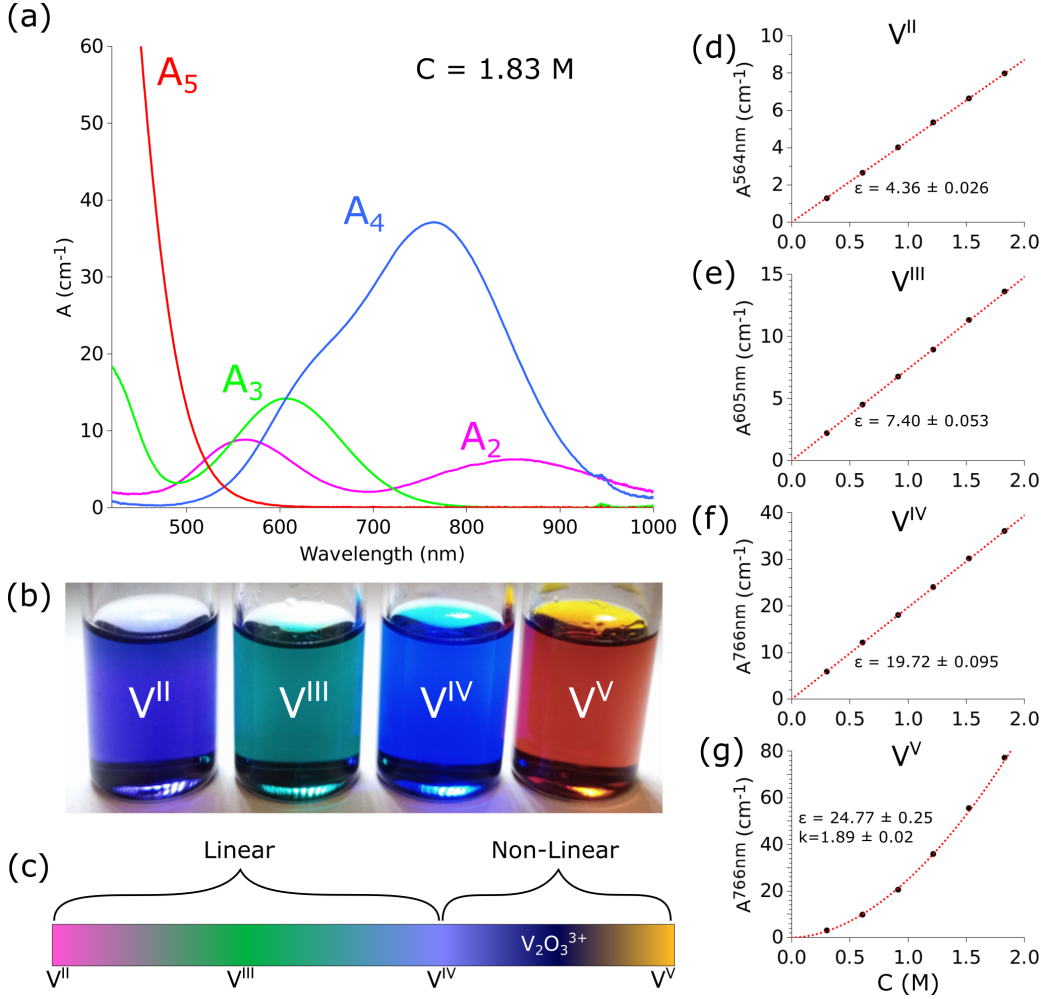


Figure 1: (a) 1.83 M reference absorbance spectra of the electrolyte solutions containing the four pure vanadium oxidation states. (b) Picture of the vials containing solutions of the pure vanadium electrolytes. The solutions were diluted when needed for visual purposes. (c) Color band representing the visual appearance of the vanadium electrolytes. The brackets indicate the locations where the spectral response is linear and non-linear. (d, e, f, g) Absorbance of V^{II} , V^{III} , V^{IV} and V^{V} extracted, respectively at 564, 605, 766, and 440 nm as a function of the concentration. The experimental points are plotted as black circles while the fit is plotted as a red dotted line.

indicate the location of the isosbestic points in which the absorbance remains constant regardless of the mole fraction. In UV-Vis spectroscopy, an isosbestic point refers to a specific wavelength at which the absorbance of the sample remains constant during a chemical reaction or a change in the sample's composition. The presence of such points suggests that the reaction occurring in the sample proceeds via a direct conversion between species, without any intermediates, e.g., reaction $\text{V}^{\text{II}} \rightleftharpoons \text{V}^{\text{III}}$.

When dealing with mixtures, the Beer-Lambert law (1) can be extended to account for multiple absorbing species. Therefore, for a binary mixture of two pure compounds A and B, with mole fractions X_A and $X_B = 1 - X_A$, the absorption spectrum is the sum of the individual absorbances of the two components

$$A_M = [\epsilon_A X_A + \epsilon_B (1 - X_A)]C \quad (3)$$

Electrolyte mixture	λ^{iso} (nm)	ϵ^{iso} ($\text{cm}^{-1}\text{M}^{-1}$)
$\text{V}^{\text{II}}/\text{V}^{\text{III}}$	722.11 ± 0.69	1.24 ± 0.001
	542.73 ± 7.03	4.06 ± 0.023
$\text{V}^{\text{III}}/\text{V}^{\text{IV}}$	608.22 ± 2.33	7.41 ± 0.05

Table 4: Wavelengths of the isosbestic points and their corresponding absorbances for the two optically linear vanadium mixtures.

where A_M is the absorbance of the mixture, ϵ_A and ϵ_B are the molar absorptivities of compounds A and B, and C is the total (vanadium) concentration. At the isosbestic point $\epsilon_A = \epsilon_B \equiv \epsilon^{\text{iso}}$ and Equation (3) reduces to

$$A_M^{\text{iso}} = \epsilon^{\text{iso}} C \quad (4)$$

In other words, at the isosbestic point the absorbance is independent of the mole fraction X_A and grows linearly with the total concentration C . Table 4 lists the isosbestic wavelengths, λ^{iso} , and the corresponding absorbance values, ϵ^{iso} , for the two optically linear vanadium mixtures. As illustrated below, the presence of isosbestic points enables the estimation of the total concentration C independently of the mole fraction X_A by directly using the values of A_M^{iso} and ϵ^{iso} in Equation (4).

The negative electrolyte ($\text{V}^{\text{II}}/\text{V}^{\text{III}}$) appears to have three isosbestic points. However, only two of them are listed in Table 4 because the third one, located around 500 nm, is too out of focus to have practical application. Equation (3) may lose validity at lower wavelengths ($\lambda < 550$) due to uncharted interactions among the vanadium compounds. This hypothesis is consistent with the findings of Loktionov et al. [30], whose results suggest the presence of additional interactions at lower wavelengths within the negative electrolyte.

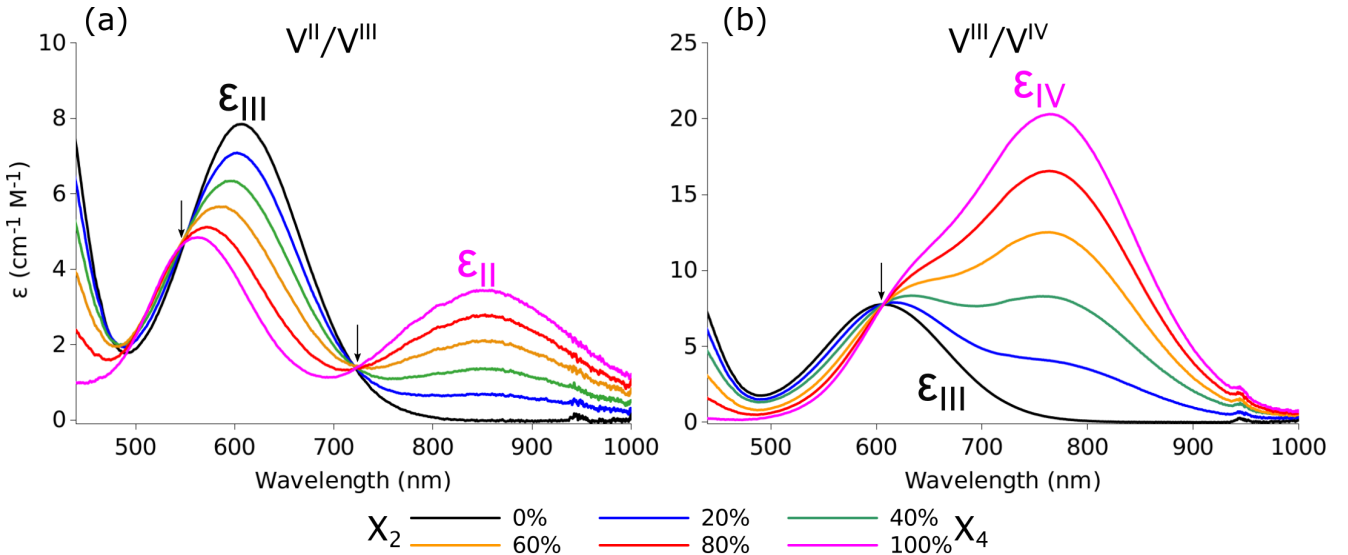


Figure 2: Molar absorptivity spectra of the $\text{V}^{\text{II}}/\text{V}^{\text{III}}$ and $\text{V}^{\text{III}}/\text{V}^{\text{IV}}$ at varying SOC/mole fractions for a total vanadium concentration $C = 1.83 \text{ M}$. The arrows indicate the location of the isosbestic points. The percentage in the legend represents the mole fractions of (a) V^{II} , which coincides with the SOC, and (b) V^{IV} , so that the black line corresponds to the molar absorption coefficient of V^{III} in both subplots.

3.2.1. Fast empirical method via linear regression

According to Equation (3), by plotting the mole fraction X_A versus the absorbance A_M at a specific wavelength and performing a linear regression analysis we could obtain a linear relationship that provided X_A in terms of A_M . However, it is important to note that despite the simplicity of this method, it may produce inaccurate results. This is primarily because the absorbance varies with the concentration C and the path length, which may be unknown or altered due to experimental conditions. For example, in the case of VRFBs, species crossover may have a significant impact on the overall concentration of vanadium ions in both the positive and negative electrolytes, thereby affecting the accuracy of the results.

We can address this problem by dividing the total mixture absorbance A_M by the absorbance at the isosbestic point A_M^{iso} , effectively merging Equations (3) and (4) into a single equation

$$\frac{A_M}{A_M^{\text{iso}}} = \frac{(\epsilon_A - \epsilon_B)X_A + \epsilon_B}{\epsilon^{\text{iso}}} \quad (5)$$

This equation can be solved explicitly for X_A to yield a linear relation of the form

$$X_A = a \frac{A_M}{A_M^{\text{iso}}} + b \quad (6)$$

with $a = \epsilon^{\text{iso}} / (\epsilon_A - \epsilon_B)$ and $b = -\epsilon_B / (\epsilon_A - \epsilon_B)$. According to this expression, X_A should vary linearly with A_M/A_M^{iso} and be independent of the total concentration C . Moreover, the total concentration C could be estimated from Equation (4) as follows

$$C = \frac{A_M^{\text{iso}}}{\epsilon^{\text{iso}}} \quad (7)$$

Hence C should grow linearly with the absorbance regardless of the mole fraction X_A , provided that the absorbance is measured at the isosbestic point.

Figures 3a and 3b show respectively the mole fractions X_2 and X_4 of the 44 calibration samples of the V^{II}/V^{III} and V^{III}/V^{IV} mixtures plotted as a function of $A_M^\lambda/A_M^{\text{iso}}$ at a particular wavelength for each mixture, along with the corresponding linear fits (6) as detailed in Table 5, using the first isosbestic wavelength reported in Table 4 for each mixture. Similarly, Figures 3c and 3d show the total concentration of vanadium ions as a function of the isosbestic absorbances A_M^{iso} along with the corresponding linear fits (7) also detailed in Table 5. The experimental points are shown as black circles, while the linear fits are plotted as red dotted lines. In these plots, all 44 calibration samples are included, meaning that the fits are performed within different vanadium concentrations. The excellent linearity observed in all cases provides strong evidence for the validity and consistency of Equations (6) and (7) across a wide range of total vanadium concentrations and mole fractions. Table 5 summarizes the correlations thus obtained with their corresponding coefficients calculated from the linear fits, as well as the estimated RMSE, commonly used for reporting the error of calibration methods.

Thus, when using the linear fits from the current calibration reported in Table 5 to determine the mole fractions, the SOC, or the total vanadium concentration of a new set of experimental data, the reported values should include, as a minimum, the uncertainty in the measurement by employing the usual notation, e.g., $X = X_{\text{exp}} \pm E_X$.

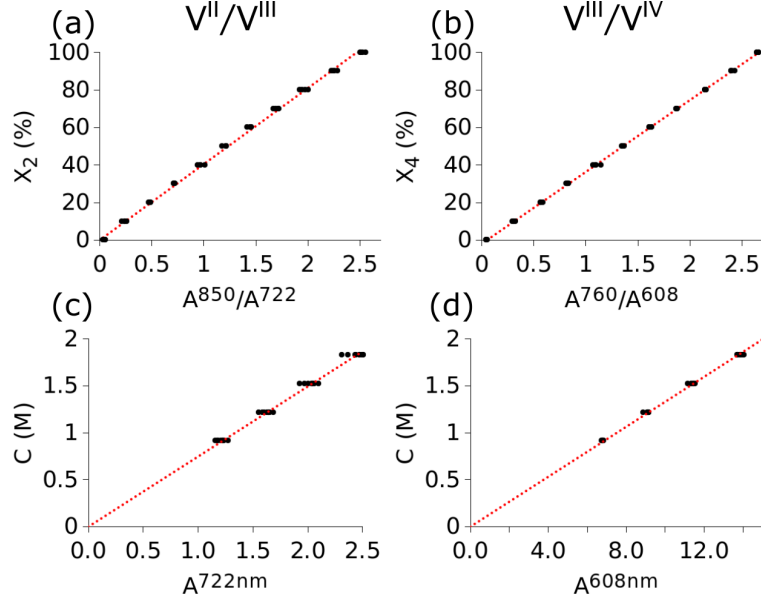


Figure 3: (a, b) Mole fractions X_2 and X_4 as a function of $A_{\text{M}}^{\lambda}/A_{\text{M}}^{\text{iso}}$ for the $V^{\text{II}}/V^{\text{III}}$ ($\lambda = 722$ nm) and $V^{\text{III}}/V^{\text{IV}}$ ($\lambda = 608$ nm) mixtures. (c, d) Total vanadium concentration as a function of $A_{\text{M}}^{\text{iso}}$ for the same mixtures. Black dots: experimental values; red dotted lines: linear fits (see Table 5). The plots display experimental results from the 44 calibration samples of each mixture, meaning that the linear regressions are performed over a wide range of total vanadium concentrations.

3.2.2. Spectral deconvolution

The spectral deconvolution method in UV-Visible spectroscopy is a technique used to separate overlapping absorption spectra of multiple components in a mixture. It involves mathematically extracting the individual contributions of each component from the observed composite spectrum, enabling the quantification of their respective concentrations or absorbances. Its application to a mixture of two pure compounds, A and B, starts by expressing the individual absorbances in terms of the known molar absorptivities, ϵ_A and ϵ_B , and the unknown molar fractions, X_A and $X_B = 1 - X_A$, and total (vanadium) concentration, C . The calibration then proceeds by fitting the best pair (X_A , C) that minimizes the sum of the error squares between the experimentally measured mixture absorbance A_{exp} and the mixture absorbance predicted by the Beer-Lambert law (3)

$$\sum_{\lambda} \{ A_{\text{exp}} - [\epsilon_A X_A + \epsilon_B (1 - X_A)] C \}^2 \quad (8)$$

As the problem involves two unknowns, a minimum of two wavelengths is required for minimization. However, in order to obtain the highest accuracy, the fit was performed over a wide spectral bandwidth (420-1000 nm) using ϵ_A and ϵ_B as reference spectra. As discussed above, the calculation range was slightly narrower than the detection range of the spectrometer (345-1033 nm). The extreme wavelengths were excluded because the signal-to-noise ratio was below the detection limit of the instrument.

Loktionov et al. [30] recently implemented this method for determining the SOC and the total concentration of vanadium ions, yielding solid results for vanadium concentrations of 0.5 M and 1 M. In this study, we extend the investigation to a broader concentration range and also

Electrolyte mixture					
	V^{II}/V^{III}		V^{III}/V^{IV}		
Variable	Linear fit	E_X	Linear fit	E_C	
X (%)	$X_2 = 40.51 \frac{A^{850}}{A^{723}}$	± 1.46	$X_4 = 38.26 \frac{A^{760}}{A^{608}} - 1.91$	± 0.52	
C (M)	$C = \frac{1}{1.34} A^{723}$	± 0.03	$C = \frac{1}{7.71} A^{608}$		± 0.015

Table 5: Linear fits for the mole fractions of V^{II} and V^{IV} versus A_M/A_M^{iso} and total vanadium concentration versus A_M^{iso} in the V^{II}/V^{III} and V^{III}/V^{IV} mixtures with indication of the corresponding RMSE errors.

incorporate the characterization of the V^{III}/V^{IV} mixture. Additionally, we report the measurement error when applying the method to calibrated samples. Figures 4a and 4b illustrate the application of spectral deconvolution to the V^{II}/V^{III} and V^{III}/V^{IV} mixtures with two representative examples. The experimental absorbance spectrum for $C = 1.83$ M and $X_A = 50\%$, with A denoting V^{II} and V^{IV} , respectively, is shown in black. The dashed lines represent the spectral contributions of each pure compound: $\epsilon_A X_A C$ and $\epsilon_B(1 - X_A)C$. According to Equation (8), the sum of the two dashed curves yields the red curve, which is the fit. Overall, the fit is accurate for all samples although a slight mismatch can sometimes be found at the lower wavelengths for the negative electrolyte, $\lambda < 600$ nm in Figure 4a. This is consistent with the suggestion stated above that the spectral response of the mixture could lose linearity at lower wavelengths [30].

For the established molar fraction and total concentration of each of the calibration samples, referred to as true values ($X_{A,T}$, C_T), spectral deconvolution was applied to obtain the so-called predicted values ($X_{A,P}$, C_P). Figures 4c, 4d, 4e, and 4f show the calibration plots for V^{II}/V^{III} (c, d) and V^{III}/V^{IV} (e, f) for the total vanadium concentration C and the mole fraction X_A . Essentially, these are scatter plots showing the predicted values versus the true values. Black dots represent the obtained results for all concentrations. In an ideal situation with perfect calibration and measurements with 100% accuracy, the predicted values would align with the true values along the bisector of the first quadrant, represented by the blue line. In practical scenarios, deviations from the blue line indicate reduced calibration accuracy and increased measurement errors. To quantify accuracy, the RMSE was computed for all concentrations, as shown in Table 6. The RMSE values were consistent over the entire concentration range, indicating uniform accuracy. Specifically, the average measurement errors for the mole fraction X_A and the concentration C were found to be 0.79% and 17 mM, respectively.

3.3. Non-linear case: V^{IV}/V^V

Figure 5 shows the absorbance spectra of the positive electrolyte V^{IV}/V^V as the SOC increases from 0% (V^{IV}) to 100% (V^V) for a total concentration $C = 1.83$ M. As indicated by the red arrow, the overall absorbance (550-1000 nm) first increases up to SOC $\approx 40\%$ (Figure 5a). Subsequently, the absorbance declines, first gradually within the 50-70% SOC range and then sharply as the SOC approaches 80-100% (Figure 5b). This observation reveals a radically different spectral response compared to that of V^{II}/V^{III} and V^{III}/V^{IV} . Another difference is that the catholyte V^{IV}/V^V

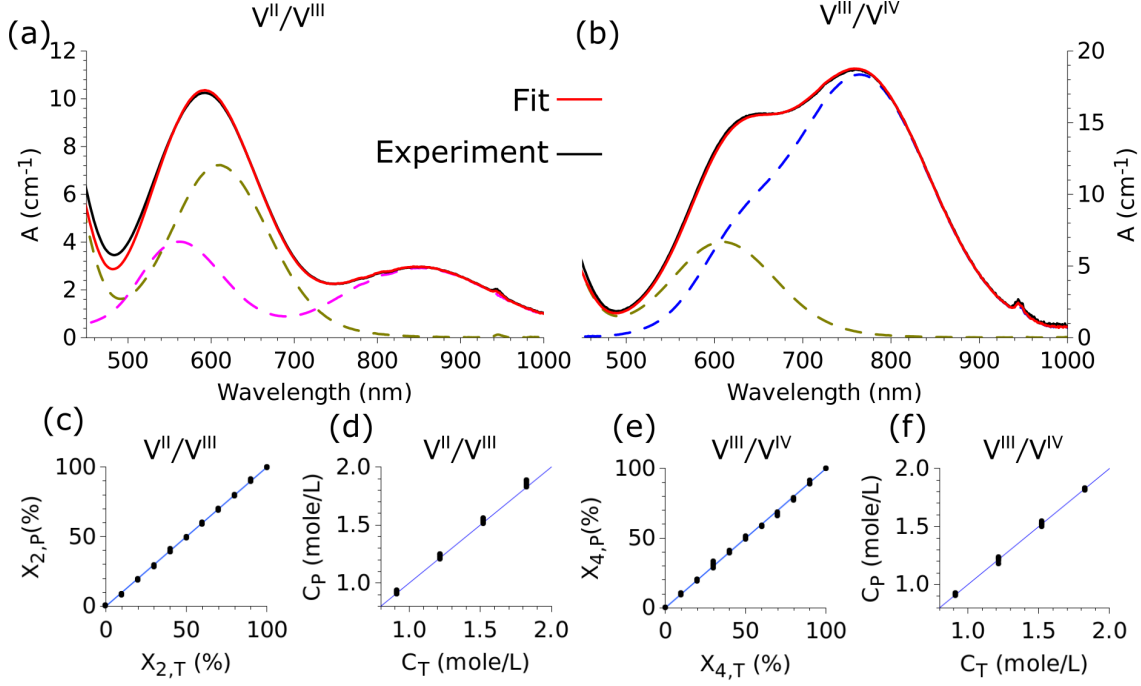


Figure 4: (a, b) Spectra of the V^{II}/V^{III} and V^{III}/V^{IV} mixtures for $X_A = 50\%$ and $C = 1.83$ M. The dashed lines represent the spectral contributions of the pure compounds V^{II}: purple, V^{III}: green, V^{IV}: blue. (c, d, e, f) Calibration curves representing the predicted values versus the true values for the mole fraction and the total concentration. The 100% accuracy line ($y = x$) is plotted in blue.

Electrolyte mixture				
	V ^{II} /V ^{III}		V ^{III} /V ^{IV}	
C (M)	E_X (%)	E_C (M)	E_X (%)	E_C (M)
1.83	1.11	0.038	0.65	0.009
1.52	0.66	0.020	1.09	0.012
1.22	0.75	0.019	0.52	0.015
0.91	0.86	0.012	0.74	0.007
Average	0.85	0.022	0.74	0.012

Table 6: Calibration results for the spectral deconvolution method showing the RMSE for the mole fraction in % and the total concentration in M for total vanadium concentrations between 0.91 M and 1.83 M.

exhibits significantly higher absorbances, reaching values as high as 65 cm⁻¹ over a wide range of wavelengths (560-850 nm) and SOCs (25-75%).

According to Blanc et al. [20], the observed high-absorbance non-linear spectral behavior can be attributed to the formation of a 1:1 stoichiometric mixed-valence complex, V₂O₃³⁺. This complex is believed to form according to the equilibrium reaction



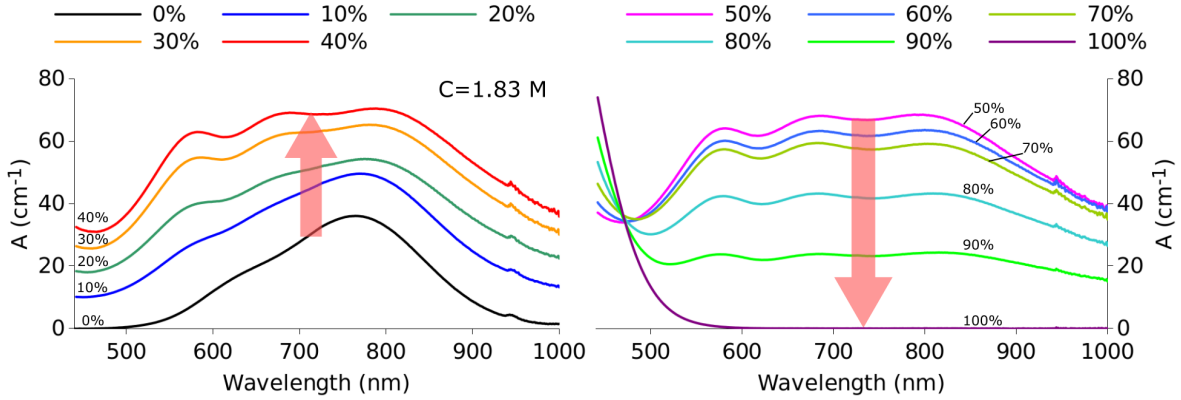


Figure 5: Absorbance spectra of the positive electrolyte $\text{V}^{\text{IV}}/\text{V}^{\text{V}}$ for different values of SOC = $X_5 = 1 - X_4$, as indicated in the curve labels, and a total vanadium concentration of $C = 1.83 \text{ M}$. Note that above 600 nm the molar absorptivity of V^{V} is virtually zero (see the bottom curve in the right subplot, SOC = 100%).

characterized by the equilibrium constant

$$K_c = \frac{C_{45}}{C_4 C_5} \quad (10)$$

written here in terms of the equilibrium concentrations of V^{IV} , V^{V} , and that of the mixed-valence complex, denoted here as C_{45} . The overall stoichiometry of reaction (9) provides the following relations between the equilibrium concentrations

$$C_4 = C_4^* - C_{45} = X_4 C - C_{45} \quad (11)$$

$$C_5 = C_5^* - C_{45} = (1 - X_4) C - C_{45} \quad (12)$$

where $C_4^* = C_4 + C_{45}$ and $C_5^* = C_5 + C_{45}$ denote the nominal concentrations of V^{IV} and V^{V} in the absence of the mixed-valence complex, i.e., in the hypothetical case $K_c = 0$. In the above equations, C_4^* and C_5^* are conveniently rewritten as the product of the total vanadium concentration $C = C_4^* + C_5^* = C_4 + C_5 + 2C_{45}$ and the nominal mole fractions $X_4 = C_4^*/C$ and $X_5 = C_5^*/C$, which are in turn related to the SOC, given by $X_5 = 1 - X_4$. For further reference, the relations between C_4 , C_5 , C_{45} , C , X_4 , X_5 , and SOC are gathered in the last column of Table 1.

Summarizing, the positive electrolyte contains 3 different compounds accounting for the total theoretical absorbance

$$A_M = A_4 + A_5 + A_{45} \quad (13)$$

where A_4 , A_5 , and A_{45} are the absorbances of V^{IV} , V^{V} , and $\text{V}_2\text{O}_3^{3+}$, respectively. With use made of Equations (1) and (2), the absorbance of the mixture can be written as

$$A_M = \epsilon_4 C_4 + \epsilon_5 C_5^k + \epsilon_{45} C_{45} \quad (14)$$

Here we assume that the mixed valence complex $\text{V}_2\text{O}_3^{3+}$ still follows the Beer-Lambert law (1), but generalize the analysis of Blanc et al. [20] by considering the non-linear dependence between A_5 and the concentration of V^{V} described by Equation(2).

Combining Equations (11), (12), and (14), we can write

$$A_M = \epsilon_4(X_4C - C_{45}) + \epsilon_5[(1 - X_4)C - C_{45}]^k + \epsilon_{45}C_{45} \quad (15)$$

Moreover, substituting Equations (11) and (12) into the equilibrium condition (10) yields a quadratic equation for C_{45} that can be solved analytically to give [20, 22]

$$C_{45} = \frac{1 - \sqrt{1 - 4\chi^2 X_4(1 - X_4)C^2}}{2\chi} \quad (16)$$

where

$$\chi = \frac{K_c}{K_c C + 1} \quad (17)$$

According to the above analysis, during the charge and discharge of the V^{IV}/V^V electrolyte the molar concentrations of the three compounds are expected to vary non-linearly with the state of charge, SOC = 1 - X_4 . This non-linear behavior poses a greater challenge for interpreting the spectra compared to the V^{II}/V^{III} and V^{III}/V^{IV} electrolytes.

It is useful to note that for wavelengths above 600 nm the molar absorptivity of V^V is virtually zero, $\epsilon_5 \approx 0$, so that Equation (15) reduces to

$$A_M^{\lambda > 600\text{nm}} = \epsilon_4(X_4C - C_{45}) + \epsilon_{45}C_{45} \quad (18)$$

which, upon substitution of C_{45} from Equations (16) and (17), yields

$$A_M^{\lambda > 600\text{nm}} = \epsilon_4X_4C + (\epsilon_{45} - \epsilon_4) \left[\frac{1 - \sqrt{1 - 4X_4(1 - X_4)(K_c C)^2 / (K_c C + 1)^2}}{2K_c / (K_c C + 1)} \right] \quad (19)$$

In this equation, K_c and ϵ_{45} are unknown constants, while C and X_4 are known parameters for each V^{IV}/V^V calibration sample. Thus, since we have an experimental database of 44 reference spectra A_{exp} for different values of C and X_4 , we can perform a multivariate function fit to find the best pair (ϵ_{45} , K_c) that, for each wavelength $\lambda > 600$ nm, minimizes the sum of the error squares

$$\sum_{\substack{C, X_4 \\ \lambda > 600\text{nm}}} (A_{\text{exp}} - A_M^{\lambda > 600\text{nm}})^2 \quad (20)$$

with the summation extending over all the 44 pairs (C , X_4) available in the V^{IV}/V^V database.

The black dots plotted in Figure 6a represent the experimentally measured absorbance at 660 nm, $A_{\text{exp}}^{660\text{nm}}$, as a function of X_4 . The red lines are the predicted absorbances resulting from the fitted values of ϵ_{45} and K_c for that particular wavelength. Figure 6b plots the coefficient of determination R^2 of the fit versus the wavelength. Details on the calculation of R^2 are given in the Supplementary Information (Section S2). Overall, the model demonstrates excellent agreement with the experimental data, with a robust and stable value of R^2 averaging $\bar{R}^2 \approx 0.99$ for $\lambda > 600$ nm. The fitted values of ϵ_{45} and K_c are represented in Figures 6c and 6d as a function of the wavelength. It is important to clarify that the observed variation of approximately $\pm 10\%$ in K_c is either a numerical artifact that results from the multivariate regression process or could be

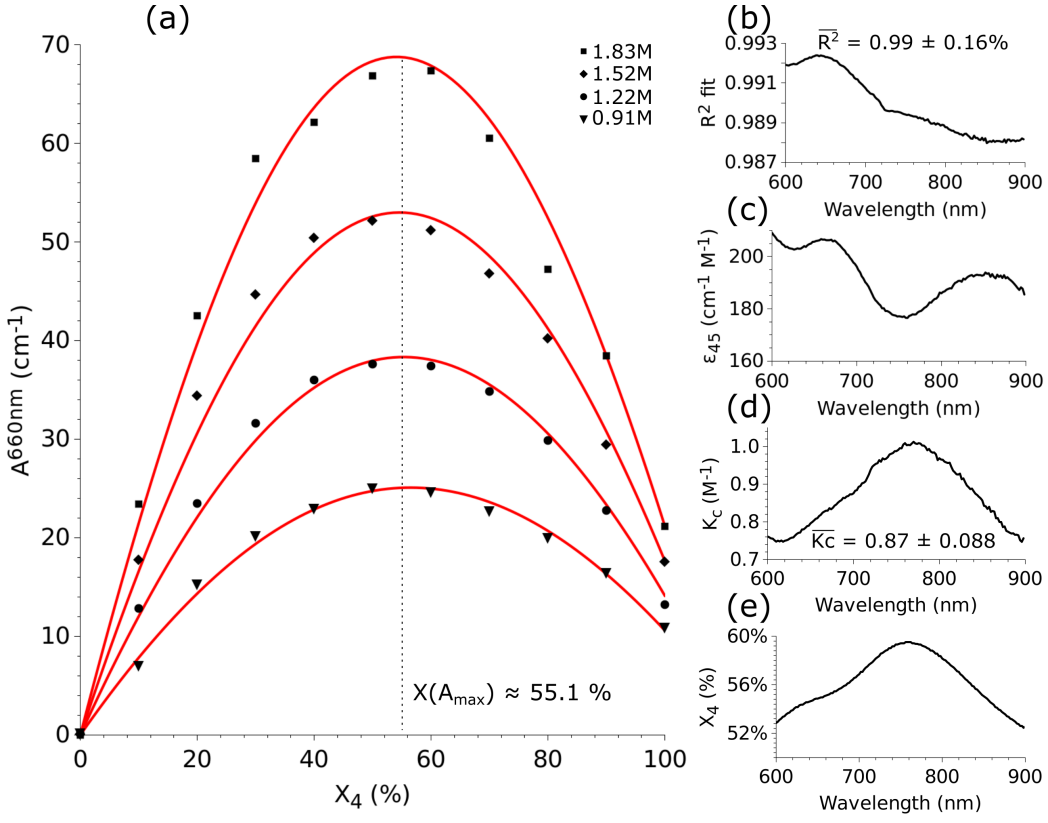


Figure 6: (a) Absorbance of the V^{IV}/V^V mixture at 660 nm as a function of X_4 for the four total vanadium concentrations under study as measured experimentally (black dots) and fitted from Equation (19) (red curves). The right plots show the fitted (b) coefficient of determination R^2 , (c) molar absorptivity of the complex, ϵ_{45} , (d) equilibrium constant, K_c along with the value of X_4 of maximum absorbance (e) as a function of the wavelength.

attributed to model limitations and experimental errors. The reaction constant K_c is a chemical property of the electrolyte, and therefore it should remain constant regardless of the wavelength sampled.

The average value of K_c indicated in the plot ($\overline{K}_c = 0.87 \pm 0.088$ M\$^{-1}\$) falls within the higher end of the range 0.2-0.8 M\$^{-1}\$ reported in the literature [20, 21, 22, 30]. Although the discrepancy is small, it could be traced back to the lower total vanadium concentrations used in the cited experiments. Additionally, by expressing the absorbance of the isolated complex in the form

$$A_{45} = \epsilon_{45} C_{45} = \epsilon_{45} K_c C_4 C_5 \quad (21)$$

it becomes clear that there is an inverse relationship between K_c and the molar absorptivity ϵ_{45} , so that the fitting could perform equally well for different pairs (ϵ_{45}, K_c) just by increasing K_c and reducing ϵ_{45} . Please note that the values of K_c reported in the literature have always been obtained indirectly, as we do in this study, without direct measurements of the complex concentration.

The last subplot, Figure 6e, shows $X_4(A_{\max})$ as a function of the wavelength. This is essentially the value of X_4 that gives maximum absorbance for a given wavelength, e.g., $X_4 = 55.1\%$ for $\lambda = 660$ nm, as shown in Figure 6a. This turning point is of practical importance as it serves as a reference marker for estimating the total concentration between charging cycles.

The results presented in this section are used below to define two calibration methods allowing to estimate the SOC = $1 - X_4$ and the total vanadium concentration C of the catholyte V^{IV}/V^V.

3.3.1. Fast empirical method

The nonlinear character of Equation (19) makes it impossible to solve it analytically for either X or C . An alternative approach involves fitting the absorbance of the mixture to a quadratic function of X_4 and C of the form

$$A_M = a_0 X_4 C + a_1 X_4 C^2 + a_2 X_4^2 C + a_3 X_4^2 C^2 \quad (22)$$

Table 7 lists the values of the fitting parameters a_i for two selected wavelengths in the range $\lambda > 600$ nm. The reported values were obtained through multivariate polynomial regression of the experimental absorbance data from the 44 calibration samples of the V^{IV}/V^V mixture at 660 nm and 760 nm. As demonstrated in the Supplementary Information (Figure S2), the quadratic fit (22) exhibits comparable performance to the theoretical equation (19) with an average R^2 of 0.99.

Fitting parameter	Wavelength λ	
	660 nm	760 nm
a_0 (M^{-1})	62.12	71.29
a_1 (M^{-2})	41.83	33.62
a_2 (M^{-1})	-50.65	-51.71
a_3 (M^{-2})	-42.63	-34.56

Table 7: Values of the fitting parameters a_i appearing in Equation (22) obtained from the absorbances of the 44 calibration samples of the V^{IV}/V^V mixture at two selected wavelengths in the range $\lambda > 600$ nm.

If the total vanadium concentration C is known, then X_4 can be obtained analytically by solving the quadratic Equation (22) to give

$$X_4 = \frac{-(a_0 C + a_1 C^2) \pm \sqrt{(a_0 C + a_1 C^2)^2 + 4 A_M (a_2 C + a_3 C^2)}}{2(a_2 C + a_3 C^2)} \quad (23)$$

which yields two possible roots (X_{4-} , X_{4+}). However, one of these roots is spurious. To elucidate which is the correct value of X_4 it is necessary to use Equation (23) with two different wavelengths (λ_1 , λ_2). By comparing the solutions obtained with these two wavelengths, the false value of X_4 can be disregarded [24]. Figure 7 illustrates the process, based on evaluating the squared differences between the roots X_{4-} and X_{4+} provided by the two wavelengths

$$D_- = (X_{4-}^{\lambda_1} - X_{4-}^{\lambda_2})^2 \quad (24)$$

$$D_+ = (X_{4+}^{\lambda_1} - X_{4+}^{\lambda_2})^2 \quad (25)$$

and selecting the root that yields the smallest difference. The value of X_4 is then computed as the arithmetic mean of the selected root obtained from both wavelengths.

As an illustrative example, Figure 7a represents the absorbance versus X_4 curves computed using Equation (22) with $C = 1.22$ M and the fitting parameters reported in Table 7 for 660 nm

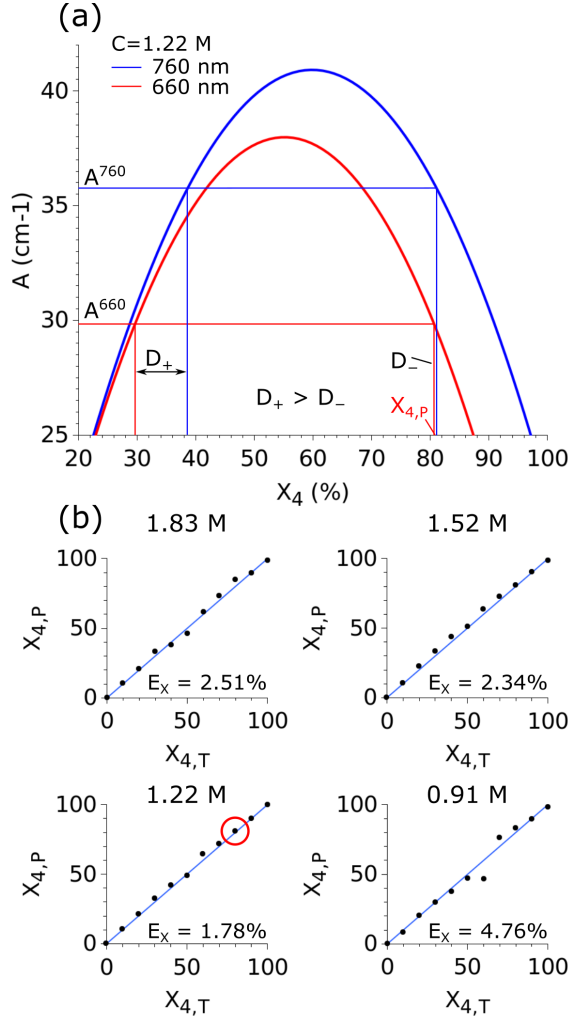


Figure 7: (a) Absorbance versus X_4 curves computed for $C = 1.21 \text{ M}$ using the quadratic fit (22) at 760 nm (blue) and 660 nm (red). The horizontal and vertical lines act as sample guidelines for the calculation of D_- , D_+ , and $X_{4,P}$, all labeled in the graph. (b) Calibration results (black dots) obtained using the fast empirical method for the four concentrations under study. The 100% accuracy line ($y = x$) is plotted in blue. The dot highlighted in red for $C = 1.22 \text{ M}$ corresponds to the sample calculation shown in (a)

and 760 nm. An illustrative example demonstrating the application of the process for determining the composition $X_{4,P}$ of a particular mixture is also provided. In this case, we used the calibration sample corresponding to $C = 1.21 \text{ M}$ and $X_{4,T} = 80\%$, plotting the experimentally measured absorbances $A_M^{660\text{nm}}$ and $A_M^{760\text{nm}}$ as horizontal lines. The intersection points of these lines with the parabolic curves represent the potential values of $X_{4,P}$. Upon analysis, it is observed that $D_- < D_+$, indicating that the correct root corresponds to the one associated with the $-$ sign. Thus, the value of $X_{4,P}$ can be obtained by averaging, in this case $X_{4,P} = (X_{4-}^{660\text{nm}} + X_{4-}^{760\text{nm}})/2 = 80.9\%$.

Figure 7b shows the calibration curves representing the predicted ($X_{4,P}$) versus the true ($X_{4,T}$) values of X_4 for each of the four concentrations within the 44 calibration samples of the $\text{V}^{\text{IV}}/\text{V}^{\text{V}}$ mixture. The error E_X is also indicated in the plots. The red circle located in the 1.22 M curve corresponds to the calibration data used as the example in Figure 7a. It is worth noting that the

method presented here is weaker than the one proposed in Section 3.2.1 for the V^{IV}/V^{III} and V^{III}/V^{IV} mixtures, since in this case X_4 and C cannot be obtained at once using only two absorbance values. Indeed, the total concentration must be either known *a-priori* or assumed, which may give rise to systematic errors over the long-term cycling of the battery due to the accumulated effect of ion crossover.

One possible way to determine the total vanadium concentration is to monitor the absorbance of the V^{IV}/V^V mixture during cycling in real time. This enables the estimation of C from the peak absorbance, A_{\max} , observed during the charge or discharge process. As previously discussed, the mole fraction at the turning point, $X_4(A_{\max})$, is well known for all wavelengths (see Figure 6e). Thus, by using the pair $(A_M, X_4) = (A_{\max}, X_4(A_{\max}))$ one can estimate the total concentration by solving the quadratic Equation (22) to give

$$C = \frac{-(a_0 X_4 + a_2 X_4^2) + \sqrt{(a_0 X_4 + a_2 X_4^2)^2 + 4 A_M (a_1 X_4 + a_3 X_4^2)}}{2(a_1 X_4 + a_3 X_4^2)} \quad (26)$$

3.3.2. Spectral deconvolution

This method is similar to the one presented in Section 3.2.2, but the equations here are slightly different due to the presence of the complex V₂O₃³⁺. The first requirement is to determine the molar absorptivity spectrum of the complex ϵ_{45} . Since this species does not appear in isolation from V^{IV} and V^V, the experimental determination of ϵ_{45} must be done indirectly. To achieve this, we can rewrite Equation (15) as

$$\epsilon_{45} = \frac{A_{\exp} - \epsilon_4(X_4 C - C_{45}) - \epsilon_5[(1 - X_4)C - C_{45}]^k}{C_{45}} \quad (27)$$

where C_{45} is evaluated from Equation (16) using the approximate value of $\chi \approx \bar{K}_c / (\bar{K}_c + 1)$ obtained from Equation (17) with the average value of the equilibrium constant reported above, $\bar{K}_c = 0.87 \text{ M}^{-1}$. The equation is applied for all the calibration samples (36 in total, disregarding the 8 samples with either X_4 or $X_5 = 0$) using A_{\exp} as the measured absorbance. The reference ϵ_{45} curve, plotted in Figure 8a, is computed by averaging over all the calibration samples (see Figure S3). Further details regarding the averaging of ϵ_{45} and the limits of the model are given in the Supplementary Information (Section S3). The high molar absorptivity of V₂O₃³⁺ is noteworthy, particularly when compared to those of V^{IV} and V^V; e.g., while ϵ_{45} reaches values as high as 200 cm⁻¹M⁻¹, ϵ_4 peaks at about 20 cm⁻¹M⁻¹ (see Figure 2)

Once the absorptivity spectrum ϵ_{45} is known, we can apply the spectral deconvolution method to any arbitrary mixture of positive electrolyte V^{IV}/V^V. The procedure involves determining the pair (X_4, C) that minimizes the sum of the error squares between the measured mixture absorbance A_{\exp} and the absorbance predicted by Equation (15), that is,

$$\sum_{\lambda} \left\{ A_{\exp} - \epsilon_4(X_4 C - C_{45}) - \epsilon_5[(1 - X_4)C - C_{45}]^k - \epsilon_{45} C_{45} \right\}^2 \quad (28)$$

where the summation ranges from 440 nm to 1000 nm, the widest wavelength range that the spectrometry system offers with a sufficient signal-to-noise ratio for the positive electrolyte.

The method proposed here includes several enhancements with respect to that proposed by Loktionov et al. [30]. A key innovation in our case is the incorporation of the power-law absorbance

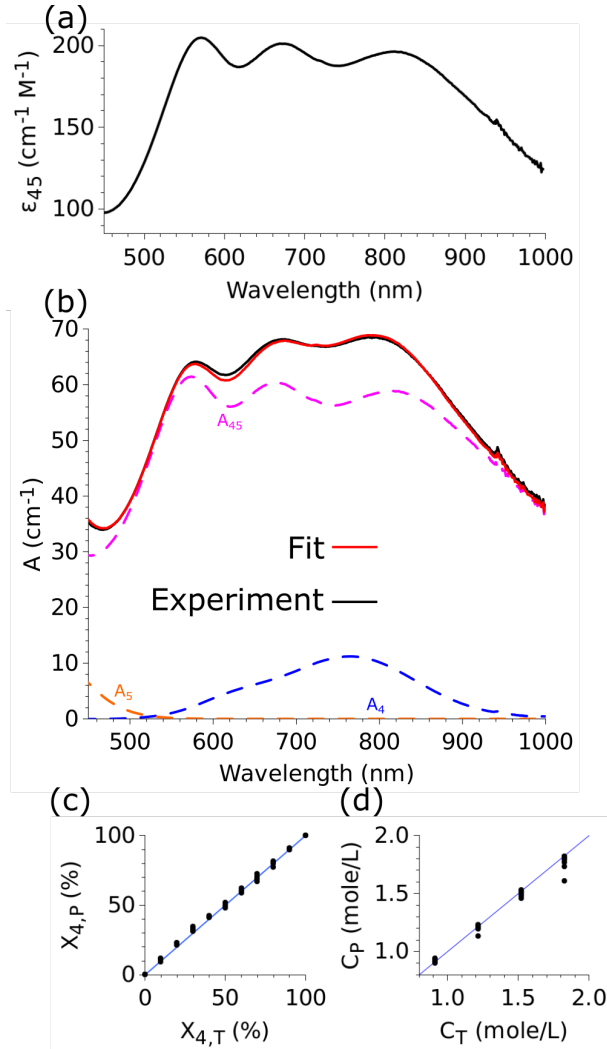


Figure 8: (a) Absorptivity spectrum of the complex $V_2O_3^{3+}$ provided by Equation (27); (b) deconvolution results for $X_4 = 50\%$ at 1.83M, with the spectral contributions of the three compounds, A_4 , A_5 , and A_{45} , shown as dashed lines; and calibration curves obtained using the spectral deconvolution method for (c) X_4 and (d) C , with the 100% accuracy line ($y = x$) plotted in blue.

versus concentration response for V^V stated in Equation (2), which translates into the nonlinear term on the right hand side of Equation (15). This generalization significantly improves the calibration results. Indeed, the use of $k = 1$ in Equation (2) leads to poor fitting results for the V^V spectrum at wavelengths lower than 600 nm. A parametric study exploring various values of k is provided in the Supplementary Information (Section S4), demonstrating that the optimal power-law exponent is $k = 2.09$. This is close to the value 1.88 reported in Figure 1, fitted using only one wavelength. Additionally, our method introduces other calibration improvements. By considering the entire range of wavelengths instead of dividing it into two ranges, we eliminate one fitting step. Moreover, the use of the analytical expressions (15) and (16) directly provides the desired values of C and X_4 for a broader range (0.91-1.83 M) of total vanadium concentrations.

Figure 8b provides an illustrative example of the spectral deconvolution process showing the

individual contribution of all compounds. The agreement is excellent, with the red curve (fitted) accurately overlapping the black curve (measured). Figures 8c and 8d show the calibration curves for X_4 and C . Finally, Table 8 indicates the RMSE errors resulting from the application of the spectral deconvolution method to both variables.

C (M)	E_X (%)	E_C (M)
1.83	2.26	0.078
1.52	1.70	0.028
1.22	1.07	0.029
0.91	1.34	0.013
Average	1.59	0.037

Table 8: RMSE error of the spectral deconvolution method of the positive electrolyte V^{IV}/V^V corresponding to the V^{IV} mole fraction, X_4 , and the total vanadium concentration, C .

4. Discussion

Figure 9 shows histogram plots of the average RMS errors E_X and E_C for the three vanadium mixtures under study, comparing the empirical and spectral deconvolution methods. Among the various vanadium mixtures, the calibrations perform slightly worse for the positive electrolyte V^{IV}/V^V . This is expected because the spectral response is significantly altered by the presence of the high absorbance complex $V_2O_3^{3+}$, as discussed in the previous section. On average, the spectral deconvolution method performs better in both measuring the total concentration C and the representative vanadium mole fractions X_i , $i = \{2, 4\}$. Additionally, no red bar is plotted for the E_C error of the the positive electrolyte since the empirical calibration measures only X_4 . The two calibration approaches differ radically in the quantity of information given to the algorithm. One the one hand, the empirical method is designed to use only a few hand-picked values while the spectral deconvolution uses the entirety of the spectrum. The deconvolution method essentially takes advantage of the whole spectrum to extract the maximum amount of information contained in it. We also expect the deconvolution approach to be more resilient to spectral distortions due to experimental errors. Such distortions can occur due to poor referencing, contaminated flow cuvettes (e.g., particles, bubbles), light scattering, change of light intensity over time, etc. These induces the spectra to be distorted or offsetted. We observed experimentally that, in such poor conditions the deconvolution was somehow able to absorb the distortions and delivered very acceptable values while the empirical methods yielded incorrect values. To delve further and assess this resilience, it would be useful to purposefully induce these distortions in a controlled manner to test the robustness of the calibration methods, but this is outside the scope of this paper. Moreover, other calibration methods could be envisioned such as correlation analysis, principal component regression, partial least square as well as advanced machine learning, such methods being already applied in other chemometrics studies [25, 39, 40].

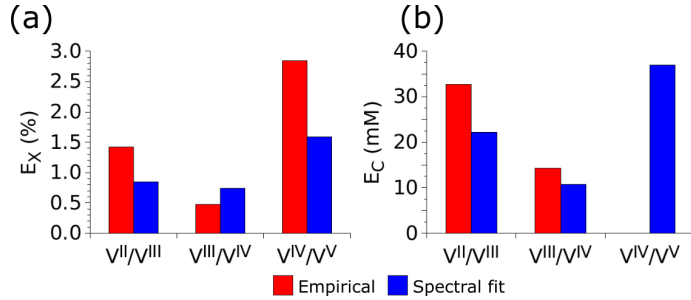


Figure 9: Histogram plots representing the average RMSE errors (a) E_X and (b) E_C for the three vanadium mixtures under study corresponding to the empirical (red) and spectral deconvolution (blue) methods.

5. Conclusions

This study presents an exhaustive overview of UV-Vis absorbance spectroscopy calibration applied to vanadium electrolytes to estimate the total vanadium concentration C and the nominal mole fraction of the mixture compounds X_i . We considered the three known mixtures of vanadium electrolytes: $\text{V}^{2+}/\text{V}^{3+}$ ($\text{V}^{\text{II}}/\text{V}^{\text{III}}$), $\text{V}^{3+}/\text{VO}_2^+$ ($\text{V}^{\text{III}}/\text{V}^{\text{IV}}$), and $\text{VO}_2^+/\text{VO}^{2+}$ ($\text{V}^{\text{IV}}/\text{V}^{\text{V}}$). In total, we provide 6 calibration methods, 3 empirical while the other 3 require computer-based fits based on spectral deconvolution. On average, we obtained errors for the mole fraction $E_X \approx 1.0\text{-}1.5\%$ and for the total concentration $E_C \approx 25\text{-}35 \text{ mM}$. Using a spectrum as the input, almost all calibrations provide both C and X_i as an output for a wide range of concentration (0.91-1.83M).

The empirical calibrations are aimed to be used in industrial applications, where a low-cost optical sensor picking up only two absorbance values could measure the SOC of the battery in real-time. This would supposedly come with a slightly worse accuracy but at a lower cost. The spectral deconvolution method is considered more powerful but computationally intensive, so it is better suited for laboratory applications where spectrometers and computers are common, but comes at a higher cost.

The data provided with this paper is publicly shared in open access repositories (GitHub) along with the Python code used to perform the calibrations. As such, anyone collecting spectral data of their vanadium electrolyte could measure the state of charge and the concentration of their electrolytes using our code and data. The main idea of this study is to provide an exhaustive, clear and useful guide to both industry and academia practitioners on how to accurately measure the total and relative concentrations of the different species present in vanadium electrolytes using UV-Vis absorbance spectroscopy. This study brings valuable insights into the constantly evolving body of knowledge on vanadium electrolytes, which will hopefully lead to the design and development of more efficient and competitive vanadium redox flow batteries in the near future.

Data availability

The calibration data and software tools developed in this work are publicly shared in the open repository https://github.com/AngeAM/SOC_Vanadium_Spectra_2023.git under the open access MIT license system. Detailed information on the metadata and the calibration scripts are given in the readme file located at the root of the repository.

Acknowledgments

We would like to acknowledge the critical hardware support provided by Micro Electrochemical Technologies S.L. (B5tec). We would also like to thank Alberto Bernaldo for his support in setting up the experimental platform, Sonia Sevilla for the help in preparing the samples, and Dr. Vanesa Muñoz-Perales for the design of the electrochemical cell. Finally, we acknowledge the support of Jesús Palma from IMDEA energía for the ICP analysis and the electrolyte supply.

Author contributions

Ange A. Maurice: Conceptualization, Methodology, Software, Validation, Formal analysis, Investigation, Resources, Data Curation, Writing - Original Draft, Visualization, Project administration, Funding acquisition. Alberto E. Quintero: Conceptualization, Methodology, Investigation, Resources, Writing - Original Draft, Supervision. Marcos Vera: Conceptualization, Formal analysis, Investigation, Resources, Writing - Review & Editing, Supervision, Project administration, Funding acquisition.

Funding

This work has been partially funded by FEDER/MICINN- Agencia Estatal de Investigación under projects TED2021-129378B-C21 and PID2019-106740RB-I00/AEI/10.13039/501100011033. A.A. Maurice acknowledges the support of an MCSF-Cofund “Energy for Future” (E4F) postdoctoral research fellowship by the Spanish Iberdrola Foundation (GA-101034297).

References

- [1] N. Zhao, F. You, Can renewable generation, energy storage and energy efficient technologies enable carbon neutral energy transition?, *Applied Energy* 279 (2020) 115889. doi:10.1016/j.apenergy.2020.115889.
- [2] A. Cunha, J. Martins, N. Rodrigues, F. P. Brito, Vanadium redox flow batteries: a technology review, *International Journal of Energy Research* 39 (7) (2015) 889–918. doi:10.1002/er.3260.
- [3] X. Z. Yuan, C. Song, A. Platt, N. Zhao, H. Wang, H. Li, K. Fatih, D. Jang, A review of all-vanadium redox flow battery durability: degradation mechanisms and mitigation strategies, *International Journal of Energy Research* 43 (13) (2019) 6599–6638. doi:10.1002/er.4607.
- [4] K. Lourenssen, J. Williams, F. Ahmadpour, R. Clemmer, S. Tasnim, Vanadium redox flow batteries: A comprehensive review, *Journal of Energy Storage* 25 (2019) 100844. doi:10.1016/j.est.2019.100844.
- [5] X. G. Yang, Q. Ye, P. Cheng, T. S. Zhao, Effects of the electric field on ion crossover in vanadium redox flow batteries, *Applied energy* 145 (2015) 306–319. doi:10.1016/j.apenergy.2015.02.038.

- [6] L. Wei, T. S. Zhao, Q. Xu, X. L. Zhou, Z. H. Zhang, In-situ investigation of hydrogen evolution behavior in vanadium redox flow batteries, *Applied Energy* 190 (2017) 1112–1118. doi:10.1016/j.apenergy.2017.01.039.
- [7] P. A. Prieto-Díaz, S. E. Ibáñez, M. Vera, Fluid dynamics of mixing in the tanks of small vanadium redox flow batteries: Insights from order-of-magnitude estimates and transient two-dimensional simulations, arXiv preprint arXiv:2305.19071 (2023).
- [8] K. W. Knehr, E. Kumbur, Open circuit voltage of vanadium redox flow batteries: Discrepancy between models and experiments, *Electrochemistry Communications* 13 (4) (2011) 342–345. doi:10.1016/j.elecom.2011.01.020.
- [9] V. Muñoz-Perales, S. E. Ibáñez, E. García-Quismondo, S. Berling, M. Vera, Exploring temperature effects in all-vanadium redox flow batteries through a validated unit-cell model, Available at SSRN 4369462 (2023). doi:10.2139/ssrn.4369462.
- [10] X. Li, J. Xiong, A. Tang, Y. Qin, J. Liu, C. Yan, Investigation of the use of electrolyte viscosity for online state-of-charge monitoring design in vanadium redox flow battery, *Applied Energy* 211 (2018) 1050–1059. doi:10.1016/j.apenergy.2017.12.009.
- [11] S. Ressel, F. Bill, L. Holtz, N. Janshen, A. Chica, T. Flower, C. Weidlich, T. Struckmann, State of charge monitoring of vanadium redox flow batteries using half cell potentials and electrolyte density, *Journal of Power Sources* 378 (2018) 776–783. doi:10.1016/j.jpowsour.2018.01.006.
- [12] P. Navalpotro, S. E. Ibáñez, E. Pedraza, R. Marcilla, A neutral ph aqueous biphasic system applied to both static and flow membrane-free battery, *Energy Storage Materials* (2023). doi:10.1016/j.ensm.2023.01.033.
- [13] J. W. Lee, M.-A. Goulet, E. Kjeang, Microfluidic redox battery, *Lab Chip* 13 (2013) 2504–2507. doi:10.1039/C3LC50499A.
- [14] V. Di Noto, K. Vezzu, G. Crivellaro, G. Pagot, C. Sun, L. Meda, I. A. Rutkowska, P. J. Kulesza, T. A. Zawodzinski, A general electrochemical formalism for vanadium redox flow batteries, *Electrochimica Acta* 408 (2022) 139937. doi:10.1016/j.electacta.2022.139937.
- [15] J.-C. M. Monbaliu, J. Legros, Will the next generation of chemical plants be in miniaturized flow reactors?, *Lab Chip* 23 (2023) 1349–1357. doi:10.1039/D2LC00796G.
- [16] J. Geiser, H. Natter, R. Hempelmann, B. Morgenstern, K. Hegetschweiler, Photometrical Determination of the State-of-Charge in Vanadium Redox Flow Batteries Part I: In Combination with Potentiometric Titration, *Zeitschrift für Physikalische Chemie* 233 (12) (2019) 1683–1694. doi:10.1515/zpch-2019-1379.
- [17] N. Roznyatovskaya, T. Herr, M. Küttinger, M. Fühl, J. Noack, K. Pinkwart, J. Tübke, Detection of capacity imbalance in vanadium electrolyte and its electrochemical regeneration for all-vanadium redox-flow batteries, *Journal of Power Sources* 302 (2016) 79–83. doi:10.1016/j.jpowsour.2015.10.021.

- [18] R. P. Brooker, C. J. Bell, L. J. Bonville, H. R. Kunz, J. M. Fenton, Determining Vanadium Concentrations Using the UV-Vis Response Method, *Journal of The Electrochemical Society* 162 (4) (2015) A608–A613. doi:10.1149/2.0371504jes.
- [19] N. H. Choi, S.-k. Kwon, H. Kim, Analysis of the Oxidation of the V(II) by Dissolved Oxygen Using UV-Visible Spectrophotometry in a Vanadium Redox Flow Battery, *Journal of The Electrochemical Society* 160 (6) (2013) A973–A979. doi:10.1149/2.145306jes.
- [20] P. Blanc, C. Madic, J. P. Launay, Spectrophotometric identification of a mixed-valence cation-cation complex between aquadioxovanadium(V) and aquaoxovanadium(IV) ions in perchloric, sulfuric, and hydrochloric acid media, *Inorganic Chemistry* 21 (8) (1982) 2923–2928. doi:10.1021/ic00138a003.
- [21] D. N. Buckley, X. Gao, R. P. Lynch, N. Quill, M. J. Leahy, Towards Optical Monitoring of Vanadium Redox Flow Batteries (VRFBs): An Investigation of the Underlying Spectroscopy, *Journal of The Electrochemical Society* 161 (4) (2014) A524–A534. doi:10.1149/2.023404jes.
- [22] N. Quill, C. Petchsingh, R. P. Lynch, X. Gao, D. Oboroceanu, D. Ní Eidhin, M. O’Mahony, C. Lenihan, D. N. Buckley, Factors Affecting Spectroscopic State-of-Charge Measurements of Positive and Negative Electrolytes in Vanadium Redox Flow Batteries, *ECS Transactions* 64 (18) (2015) 23–39. doi:10.1149/06418.0023ecst.
- [23] X. Gao, R. P. Lynch, M. J. Leahy, D. N. Buckley, Spectroscopic Study of Vanadium Electrolytes in Vanadium Redox Flow Battery (VRFB), *ECS Transactions* 45 (26) (2013) 25–36. doi:10.1149/04526.0025ecst.
- [24] C. Petchsingh, N. Quill, J. T. Joyce, D. N. Eidhin, D. Oboroceanu, C. Lenihan, X. Gao, R. P. Lynch, D. N. Buckley, Spectroscopic Measurement of State of Charge in Vanadium Flow Batteries with an Analytical Model of V^{IV} - V^V Absorbance, *Journal of The Electrochemical Society* 163 (1) (2016) A5068–A5083. doi:10.1149/2.0091601jes.
- [25] L. Liu, J. Xi, Z. Wu, W. Zhang, H. Zhou, W. Li, X. Qiu, State of charge monitoring for vanadium redox flow batteries by the transmission spectra of V(IV)/V(V) electrolytes, *Journal of Applied Electrochemistry* 42 (12) (2012) 1025–1031. doi:10.1007/s10800-012-0477-2.
- [26] Z. Tang, D. S. Aaron, A. B. Papandrew, T. A. Zawodzinski, Monitoring the State of Charge of Operating Vanadium Redox Flow Batteries, *ECS Transactions* 41 (23) (2012) 1–9. doi:10.1149/1.3697449.
- [27] W. Zhang, L. Liu, L. Liu, An on-line spectroscopic monitoring system for the electrolytes in vanadium redox flow batteries, *RSC Advances* 5 (121) (2015) 100235–100243. doi:10.1039/C5RA21844F.
- [28] K.-H. Shin, C.-S. Jin, J.-Y. So, S.-K. Park, D.-H. Kim, S.-H. Yeon, Real-time monitoring of the state of charge (SOC) in vanadium redox-flow batteries using UV–Vis spectroscopy in operando mode, *Journal of Energy Storage* 27 (2020) 101066. doi:10.1016/j.est.2019.101066.

- [29] A. Tang, J. Bao, M. Skyllas-Kazacos, Thermal modelling of battery configuration and self-discharge reactions in vanadium redox flow battery, *Journal of Power Sources* 216 (2012) 489–501. doi:10.1016/j.jpowsour.2012.06.052.
- [30] P. Loktionov, R. Pichugov, D. Konev, M. Petrov, A. Pustovalova, A. Antipov, Operando UV/Vis spectra deconvolution for comprehensive electrolytes analysis of vanadium redox flow battery, *Journal of Electroanalytical Chemistry* 925 (2022) 116912. doi:10.1016/j.jelechem.2022.116912.
- [31] P. W. Atkins, J. de Paula, *Physical chemistry*, 10th Edition, Oxford University Press, 2014.
- [32] D. C. Harris, *Quantitative chemical analysis*, 9th Edition, W. H. Freeman and Company, 2015.
- [33] D. A. Skoog, F. J. Holler, S. R. Crouch, D. M. West, *Fundamentals of analytical chemistry*, 9th Edition, Cengage Learning, 2013.
- [34] F. J. Oldenburg, M. Bon, D. Perego, D. Polino, T. Laino, L. Gubler, T. J. Schmidt, Revealing the role of phosphoric acid in all-vanadium redox flow batteries with DFT calculations and in situ analysis, *Phys. Chem. Chem. Phys.* 20 (36) (2018) 23664–23673, publisher: The Royal Society of Chemistry. doi:10.1039/C8CP04517H.
- [35] Y. Ashraf Gandomi, D. Aaron, Z. Nolan, A. Ahmadi, M. Mench, Direct Measurement of Crossover and Interfacial Resistance of Ion-Exchange Membranes in All-Vanadium Redox Flow Batteries, *Membranes* 10 (6) (2020) 126. doi:10.3390/membranes10060126.
- [36] L. G. Bannard, J. D. Burton, The spectrophotometric determination of vanadium(V) with 3,3-dimethylnaphthidine, *The Analyst* 93 (1104) (1968) 142–147. doi:10.1039/AN9689300142.
- [37] T. G. Mayerhöfer, S. Pahlow, J. Popp, The bouguer-beer-lambert law: Shining light on the obscure, *ChemPhysChem* 21 (18) (2020) 2029–2046. doi:10.1002/cphc.202000464.
- [38] O. Nolte, R. Geitner, M. D. Hager, U. S. Schubert, Ir spectroscopy as a method for online electrolyte state assessment in rfbs, *Advanced Energy Materials* 11 (28) (2021) 2100931. doi:10.1002/aenm.202100931.
- [39] S. Guo, J. Popp, T. Bocklitz, Chemometric analysis in Raman spectroscopy from experimental design to machine learning-based modeling, *Nature Protocols* 16 (12) (2021) 5426–5459. doi:10.1038/s41596-021-00620-3.
- [40] C. A. Meza Ramirez, M. Greenop, L. Ashton, I. u. Rehman, Applications of machine learning in spectroscopy, *Applied Spectroscopy Reviews* 56 (8-10) (2021) 733–763. doi:10.1080/05704928.2020.1859525.

Supplementary Information to

A comprehensive guide for measuring total vanadium concentration and state of charge of vanadium electrolytes using UV-Visible spectroscopy

Ange A. Maurice^a, Alberto E. Quintero^{a,b}, Marcos Vera^a

^aDepartamento de Ingeniería Térmica y de Fluidos, Universidad Carlos III de Madrid, Avd. de la Universidad 30, Leganés, 28911, Madrid, Spain

^bR&D Department, Micro Electrochemical Technologies, Leganés, 28918, Madrid, Spain

S1. Preparation of V^{III} and V^{IV} via spectrophotometric titration

This part describes the preparation of pure V^{III} and V^{IV} through spectrophotometric titration outlined in Section 2.1. Spectrophotometric titration is a quantitative analytical technique that combines the principles of spectrophotometry and titration. This technique involves measuring the absorbance of a sample at specific wavelengths to determine the concentration of a particular substance. In the case of vanadium electrolytes, the titration process involves the gradual oxidation or reduction of the sample, which alters its light-absorbing properties.

Figure S1 illustrates the application of spectrophotometric titration in monitoring the charging process of the V^{III}/V^{IV} electrolyte. The absorbance A^λ is plotted as a function of time at specific wavelengths both for the positive side (oxidation, $\lambda = 470$ nm) in Figure S1a and the negative side (reduction, $\lambda = 850$ nm) in Figure S1b. The inflection points observed in the curves indicate the precise moment when the electrolyte consists solely of one oxidation state, signifying the transition state, or endpoint, from one electrolyte type to another. These distinct minima serve as reference points to prepare the reference electrolytes, enabling accurate analysis and comparison.

S2. Empirical fitting of the positive electrolyte and calculation of R^2

This part details the fitting of the positive electrolyte absorbance using the empirical method outlined in Section 3.3.1 as well as the calculation of R^2 (also used in 3.3, Figure 6b). Figure S2a

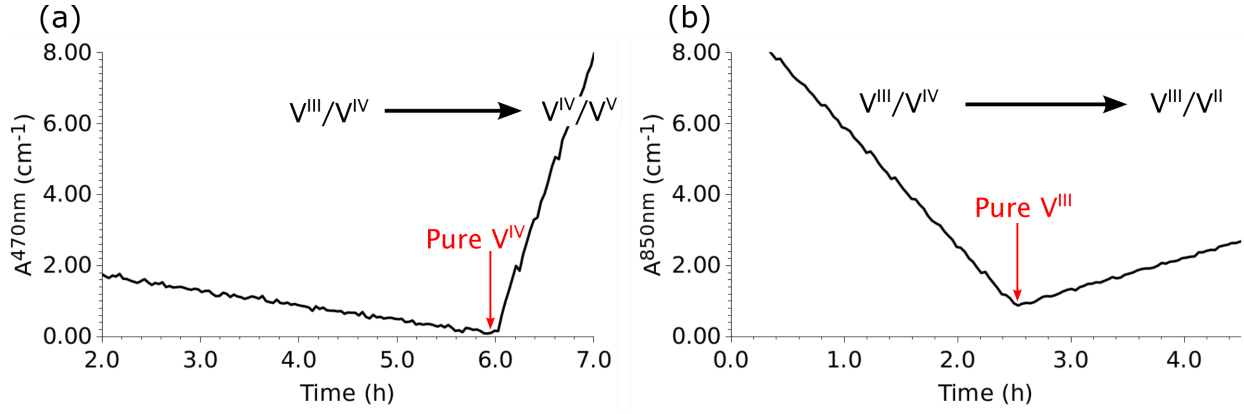


Figure S1: Plots of the absorbance A^λ as a function of time at specific wavelengths during the charging process of the V^{III}/V^{IV} electrolyte for (a) the positive side and (b) the negative side. A distinct inflection point can be observed in each subplot indicating the transition to a different electrolyte mixture.

shows the absorbance of V^{IV}/V^V at 660 nm as a function of X_4 for the four concentrations. The black dots are the experimental points (A_{exp}) and the red line is the fitted curve (A_p) obtained from Equation (22). As pointed out in the main text, the empirical fit performs as well as the analytical fit shown in Figure 6. This is further confirmed by the high value of R^2 shown in Figure S2b. The coefficient of determination is calculated at each wavelength following its classical definition

$$R^2 = 1 - \frac{SS_{\text{res}}}{SS_{\text{tot}}}$$

in terms of the sum of squares of residuals

$$SS_{\text{res}} = \sum_{C,X_4} (A_{\text{exp}} - A_p)^2$$

where A_p denote the predicted absorbance values (plotted as red lines in Figure 6a and Figure S2a), and the total sum of squares

$$SS_{\text{tot}} = \sum_{C,X_4} (A_{\text{exp}} - \overline{A_{\text{exp}}})^2$$

defined as the sum over all squared differences between the observations and their overall mean.

S3. Averaging of ϵ_{45}

This section describes the procedure for determining the molar absorptivity of the complex, ϵ_{45} , used in the spectral deconvolution of the positive electrolyte as described in Section 3.3.2 of the

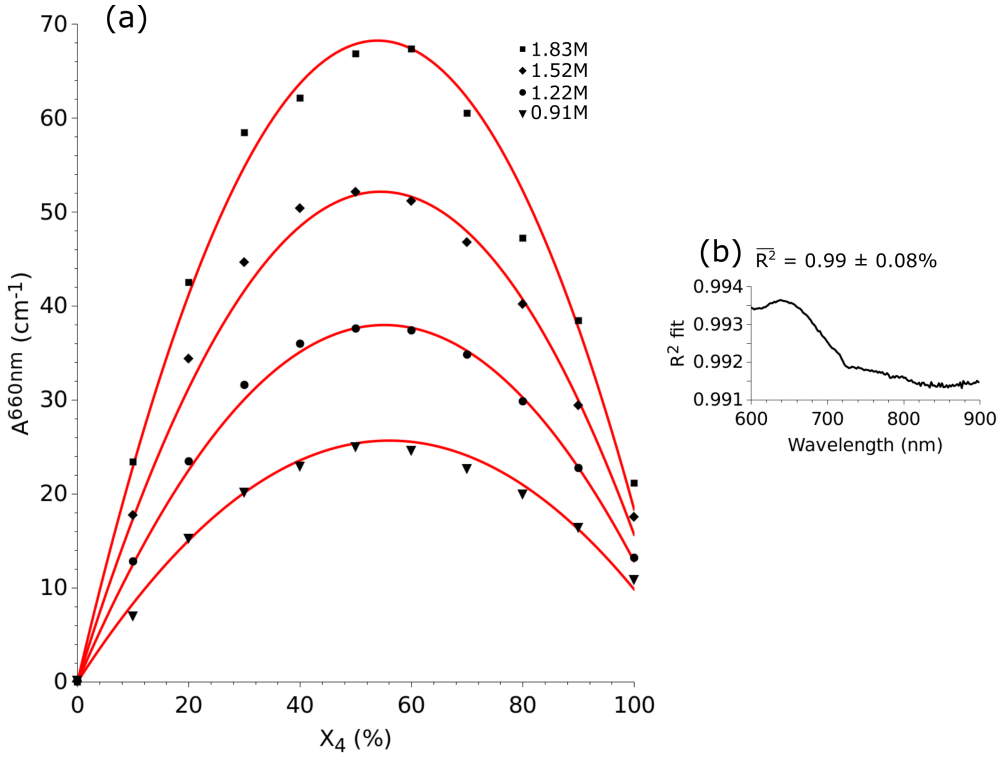


Figure S2: (a) Absorbance of the $\text{V}^{\text{IV}}/\text{V}^{\text{V}}$ mixture at 660 nm as a function of X_4 for the four total vanadium concentrations under study as measured experimentally (black dots) and fitted from the empirical Equation 22 (red curves). The right plot show the fitted (b) coefficient of determination R^2 as a function of the wavelength.

main text. Figure S3 shows in gray the calculated absorptivities of the complex ϵ_{45} obtained from Equation (27) for all 36 calibration samples of the positive electrolytes. In order to exclude samples where the complex is absent, those with $X_4 = 0\%$ or 100% were omitted. According to the model assumptions, only one unique ϵ_{45} curve should be associated with the complex, regardless of the values of X or C . The average of the gray curves is arbitrarily chosen as a reference (depicted as the red curve) for the calibration process, yielding satisfactory deconvolution results as highlighted in the main text (with a root mean square error $E_X \approx 1\%$). Nonetheless, the relatively high observed dispersion ($\approx 3 - 12\%$) suggests that the absorbance model described in this study still has its limitations. Unknown non-linear effects might be at play, opening the door for potential improvements of the absorbance model in future studies.

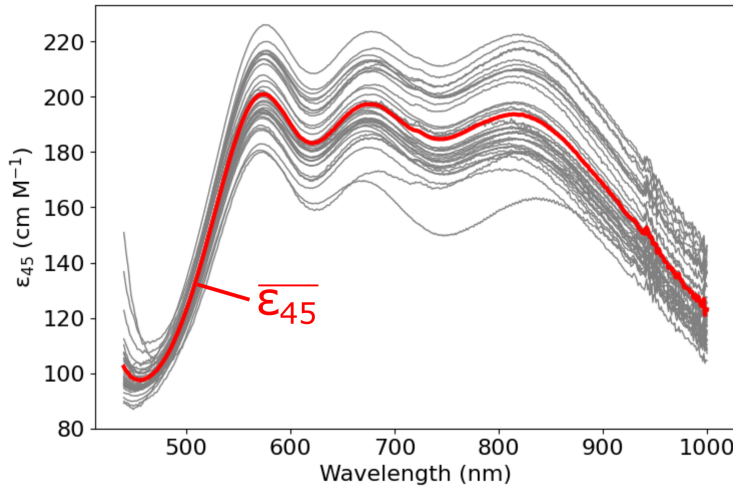


Figure S3: Molar absorptivity of the complex ϵ_{45} computed using Equation (27) for each calibration sample of the positive electrolyte (gray lines), and average absorptivity (red line) used as reference for the calibration.

S4. Parametric study for the spectral deconvolution of the positive electrolyte

This section presents a parametric study aimed at determining the optimal value of the power-law exponent k that minimizes the overall experimental error in the spectral deconvolution of the positive electrolyte presented in Section 3.3.2 of the main text. Figure S4 illustrates the result of the study by plotting the product of the RMSE errors, E_{X_4} and E_C , as a function of the factor k involved in Equations (2), (27), and (28). Notably, the figure exhibits a clear minimum at $k = 2.09$, indicating that this value represents the optimal choice for the deconvolution process. In fact, this

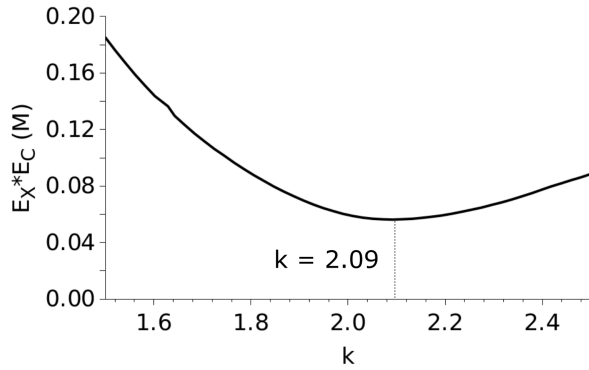


Figure S4: Product of E_{X_4} and E_C as a function of k for the spectral deconvolution of the positive electrolyte. A clear minimum is reached for $k = 2.09$.

is the value used in the results presented in Figure 8 and Table 8. It is worth noting that 2.09 is consistent with the value $k = 1.88$ indicated in Figure 1g, computed using a single wavelength of 440 nm.